Forever young: how AHL15 delays developmental phase transitions to prevent ageing in plants

Luden, T.

Chapter 4

The plant longevity gene *AHL15* inhibits leaf senescence by repressing *ORESARA1* and cytokinin degradation

Thalia Luden[1], Petra Amakorová[3], Ondřej Novák[3], Salma Balazadeh[2], Remko Offringa[1]

[1] Plant Developmental Genetics and [2] Plant Stress Biology, Institute of Biology Leiden, Leiden University, Sylviusweg 72, 2333 BE Leiden, the Netherlands
[3] Laboratory of Growth Regulators, Faculty of Science, Palacký University and Institute of Experimental Botany, The Czech Academy of Sciences, CZ-77900 Olomouc, Czech Republic

Abstract

The *Arabidopsis thaliana* (Arabidopsis) *AT-HOOK MOTIF NULCEAR LOCALIZED15 (AHL15)* gene is associated with various longevity phenotypes and extends the life span of plants when overexpressed. Here, we show that, in addition to previously described longevity phenotypes, constitutive overexpression of *AHL15* in Arabidopsis delays leaf senescence, whereas *ahl15* loss-of-function accelerates this process. Dexamethasone-induced nuclear localization of AHL15-GR during dark-triggered senescence results in a stay-green phenotype and represses the expression of several early senescence-associated genes. Among these, the *ORESARA1* (*ORE1*) locus is directly bound by AHL15, implying a direct repressive effect of AHL15 on senescence. In addition, we show that AHL15 acts by directly repressing the expression of several *CYTOKININ OXIDASE* (*CKX*) genes involved in cytokinin inactivation, resulting in a delayed degradation of cytokinins during dark-induced senescence. Cytokinins are known to inhibit senescence, and together with the downregulation of *ORE1* expression, this explains the repressive effect of *AHL15* on senescence.

Keywords: AHL15, leaf senescence, ORESARA1, Cytokinin, CKX

Introduction

Leaf senescence is the process during which the photosynthetic machinery of leaves is catabolized and recycled for use in other parts of the plant (Lim et al., 2007a; Schippers et al., 2015; Guo et al., 2021). It is the final developmental stage of leaves, and its progression is tightly controlled by various transcription factors (TFs) among which the NAC-family TFs ORESARA1 (ORE1) and NAC-LIKE, ACTIVATED BY AP3/PI (NAP) (Guo and Gan, 2006; Kim et al., 2009; Qiu et al., 2015). Loss-of-function of *ore1*, *nap,* or other positive regulators of senescence results in a stay-green phenotype (Guo and Gan, 2006; Kim et al., 2009), and ORE1 regulates the transcription of numerous genes in the senescence pathway (Balazadeh et al., 2010). Upon initiation of senescence, genes involved in chlorophyll degradation (also called chlorophyll catabolic genes) are upregulated by ORE1, NAP, and other TFs in the senescence pathway, and together the resulting enzymes degrade chlorophyll (Chl) into smaller molecules that can be exported to other tissues in the plant, resulting in the characteristic yellowing of senescent leaves (Qiu et al., 2015; Yang et al., 2015; Woo et al., 2019). The relocation of nutrients from older leaves to other parts of the plant can help regulate the availability and distribution of nutrients, and thereby increases a plant's chance of survival in times of nutrient scarcity (Schippers et al., 2015). However, when senescence negatively impacts the overall quality of a crop, such as in leafy vegetables or in ornamental plants, delayed senescence can be a desirable trait. Therefore, achieving improved control of leaf senescence is essential for enhancing crop quality.

Senescence can be induced by various factors, including leaf age, dark incubation, nutrient shortage, and the application of hormones such as ethylene, jasmonic acid (JA), abscisic acid (ABA), salicylic acid (SA), or strigolactones (SL) (Woo et al., 2019). Ethylene induces a signaling cascade that activates the TF ETHYLENE INSENSITIVE 3 (EIN3), which in turn promotes transcription of *ORE1* and *NAP* (Li et al., 2013; Kim et al., 2014), and dark incubation induces transcription of both *ORE1* and *EIN3* via PHYTOCHROME INTERACTING FACTOR4 (PIF4) and PIF5 (Song et al., 2014). In monocarpic plants, flowering also triggers leaf senescence, allowing the relocation of nutrients from leaves to seeds and thereby enhancing the offspring's chances of survival (Thomas, 2013). For example, in *Arabidopsis thaliana* (Arabidopsis), the whole plant senesces within a few weeks after flowering. This process is controlled by several TFs, among which MYB2 and FRUITFULL (FUL), and coincides with reduced production of the hormone cytokinin (CK) (Guo and Gan, 2011; Balanzà et al., 2018).

In contrast to most other plant hormones that induce senescence, CKs inhibit leaf senescence: exogenous CK application significantly delays leaf senescence (Richmond et al., 1957; Gan and Amasino, 1995). The senescence-inhibiting activity of CK is mediated by the CK receptor ARABIDOPSIS HISTIDINE KINASE 3 (AHK3), which phosphorylates ARABIDOPSIS RESPONSE REGULATOR 2 (ARR2) upon CK perception (Kim et al., 2006). ARR2 then promotes expression of *CYTOKININ RESPONSE FACTOR 6* (*CRF6*), a TF that negatively regulates leaf senescence via an unknown mechanism (Zwack et al., 2013). Loss-of-function mutants of *ahk3* show accelerated senescence phenotypes and the senescence-inhibiting effect of CK treatment is reduced in these plants as a result of their weakened ability to transduce CK signals (Kim et al., 2006). A similar phenotype can be seen in *crf6* mutants (Zwack et al., 2013).

CKs are synthesized predominantly by enzymes of the ISOPENTENYL TRANSFERASE (IPT) and LONELY GUY (LOG) families. IPT-family enzymes are responsible for adding a prenyl group to N^6 of ATP or ADP (Kakimoto, 2001; Takei et al., 2001). Additional enzymes such as CYP735A are involved in making changes to this prenyl group, thereby producing precursors to different CK variants (Argueso and Kieber, 2024). Biological activation of these CK precursors relies on the removal of the riboside group by LOG-family enzymes, which are highly redundant and of which LOG7 and LOG8 appear to be the most important in Arabidopsis (Kuroha et al., 2009; Tokunaga et al., 2012). CK degradation is predominantly accomplished by enzymes of the CYTOKININ OXIDASE/DEHYDROGENASE (CKX) class. CKX enzymes irreversibly cleave off the N^6 side chains from active CKs, thereby inactivating them permanently (Galuszka et al., 2000; Schmülling et al., 2003). Knockout of the rice *ckx11* gene causes a delay in leaf senescence, indicating that reduced CK degradation negatively affects senescence (Zhang et al., 2021a). On the other hand, overexpression of *LOG4* delays leaf senescence in Arabidopsis (Kuroha et al., 2009), and expression of the *Agrobacterium tumefaciens IPT* gene under the senescence-specific *SAG12* promoter delays leaf senescence in several crops (Gan and Amasino, 1995; Jordi et al., 2000; McCabe et al., 2001). Thus, leaf senescence can be regulated by controlling the expression of the CK biosynthesis genes of the *IPT* and *LOG* families and by regulating the expression of the CK-degrading *CKX* genes.

While CK plays an important role in senescence, the regulatory mechanisms that control CK-mediated inhibition of senescence remain elusive. So far, only two TFs that regulate CK levels during senescence have been identified: MYB2 and NAP. In wild type plants, *IPT* expression in the leaf is silenced by MYB2, whose expression increases with progressing age (Guo and Gan, 2011). It

was shown that *MYB2* expression in Arabidopsis and the legume *Caragana intermedia* can be repressed by proteins of the S40 family, and overexpression of *S40*-family genes results in enhanced CK levels and a stay-green phenotype (Yang et al., 2022). The expression of *CRF6* also decreases in older leaves through an unknown mechanism (Zwack et al., 2013). At the same time, *CKX3* expression is induced by the senescence-promoting TF NAP, resulting in enhanced CK degradation (Hu et al., 2021). The repression of *CKX* expression by NAP was observed in Arabidopsis and in Chinese cabbage, indicating that this pathway is conserved (Hu et al., 2021; Li et al., 2023). These results show a clear link between CK and age-induced senescence, but additional regulatory mechanisms that control the expression of CK biosynthesis- and degrading genes during the senescence process remain to be identified.

Previously, we identified the Arabidopsis gene *AT-HOOK MOTIF NUCLEAR LOCALIZED15* (*AHL15*) as a regulator of plant longevity: overexpression of *AHL15* in Arabidopsis resulted in an increased life span and flowering time and an enhanced vegetative development of axillary meristems, branching and secondary growth, whereas *ahl15* loss-of-function or perturbed *ahl* function reduced all these aspects (Karami et al., 2020; Rahimi et al., 2022b). CK levels were increased in stems of *AHL15* overexpressing plants, explaining the enhanced secondary growth and branching phenotypes in these plants (Rahimi et al., 2022b). In Arabidopsis, the *AHL* gene family is comprised of 29 members that are subdivided into two clades (clade A and B) (Zhao et al., 2014). Previous research has demonstrated that members of the clade A *AHL* subfamily, which includes *AHL15*, exhibit a high level of functional redundancy (Yun et al., 2012; Zhao et al., 2013; Karami et al., 2020). Lim et al. (2007b) showed that overexpression of the clade A member *AHL27* represses leaf senescence, whereas recently, the clade B member *AHL9* has been identified as a promoter of leaf senescence, suggesting that clade A and B AHLs may operate antagonistically (Lim et al., 2007b; Zhou et al., 2022).

Here, we show that similar to *AHL27,* overexpression of *AHL15* delays leaf senescence, while loss-of-function *ahl15* mutants exhibit early senescence. Our results show that the expression of several senescence marker genes is repressed when AHL15 activity is induced and that AHL15 directly binds to the *ORESARA1* locus, indicating that AHL15 directly inhibits the senescence developmental program. Additionally, we found that AHL15 binds upstream of the *CKX2*, *CKX3*, and *CKX5* genes, and that induction of AHL15 activity leads to nearly complete silencing of their expression. This silencing coincides with a slower decrease in CK levels during dark-induced senescence. Together,

our data reveal that AHL15 delays the senescence program through parallel pathways: By repressing expression of *ORE1* and by repressing *CKX* expression and subsequent CK degradation.

Results

AHL15 overexpression delays the onset of leaf senescence

Given that overexpression of *AHL15* extends overall plant longevity and because delayed senescence has previously been reported for *AHL27* overexpressing lines (Lim et al., 2007b), we tested whether a similar late-senescence phenotype could also be observed in *p35S:3xFLAG-AHL15* plants (hereafter referred to as *AHL15* OX). At 42 days after germination, the older leaves of Col-0 (wild type) and *ahl15* knockout plants started to senesce, whereas leaves of the same age in *3xFLAG-AHL15* overexpressing lines stayed green, indicating that senescence may indeed be delayed by *AHL15* overexpression (Figure 1A). To monitor this in more detail, we harvested fifth leaves of different plants at 21, 24, 27, 30, 34, and 36 days of emergence and used images of these leaves to measure the chlorophyll content through a recently developed colorimetric assay (Figure 1B). This assay measures the pixel intensity value in Red, Green, and Blue channels of digital images, which can be used to calculate the normalized Red value (Rn; Red/(Red+Green+Blue)). Previously, we have shown that this correlates well with the total Chl content of leaves (this thesis chapter 3). The progression of senescence in the fifth leaf was also delayed in *AHL15* OX plants, whereas its onset was not affected in *ahl15* loss-of-function plants (Figure 1). Next, we tested whether this delayed senescence was also visible upon senescence induction by dark incubation. In *AHL15* OX plants, dark-induced senescence of the fifth leaf was significantly delayed compared to wild type, which was reflected by both the Rn value and the total Chl content (Figure 2). In addition, *ahl15* loss-of-function plants showed a mild but significant reduction in Rn value and total Chl content compared to Col-0, supporting our finding that *AHL15* inhibits leaf senescence.

Overexpression of *AHL15* and other clade-A *AHLs* generally delays flowering time and vegetative phase change (Karami et al., 2020; Rahimi et al., 2022a). To evaluate the effects of *AHL15* overexpression on the senescence phenotype independently of other developmental processes, we used a dexamethasone (DEX)-inducible *p35S:AHL15-GR* line in which the AHL15-GR fusion protein translocates to the nucleus upon DEX treatment (Karami et al., 2020). To induce AHL15 activity in this line simultaneously with the senescence process, we

added 10 µM DEX to the MES buffer on which leaves were floated during the dark incubation period. DEX-treated *p35S:AHL15-GR* leaves showed a similar delayed senescence phenotype as *AHL15* OX leaves, whereas mock-treated

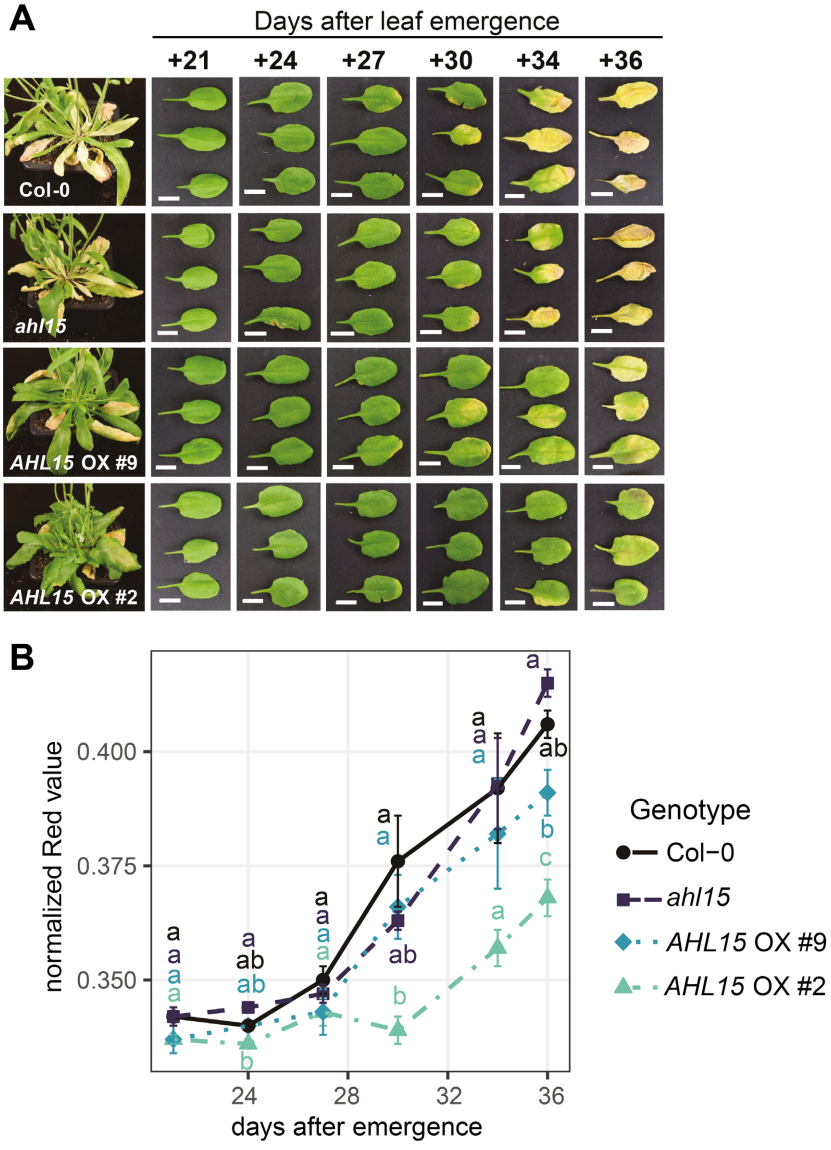

Figure 1: Progression of senescence in the fifth leaf of wild-type (Col-0), *ahl15*, and *AHL15 OX* (*p35S:3xFLAG-AHL15*) plants. **A**: images of 42 day-old plants grown at long day conditions (left) and the fifth leaf at progressing days after emergence (right). White bars represent 1 cm. Plants were grown in 5 cm wide pots. **B**:The chlorophyll content was quantified based on the images in **A** as the normalized Red value (Rn), with four leaves per time point. Groups were compared at each time point by Kruskall-Wallis test, and letters indicate significance groups; groups with the same letter do not differ significantly from one another (n = 4; $p<0.05$).

p35S:AHL15-GR leaves senesced like wild-type leaves (Figure 3A-C).

We next investigated the effect of DEX-induced AHL15-GR nuclear localization on the expression of senescence-associated genes after increasing periods of dark incubation. Based on the Rn value and total Chl content of leaves incubated in the dark over a five-day period, significant differences between DEX-induced and non-induced leaves (DEX-treated vs mock-treated *p35S:AHL15-GR,* or DEX-treated Col-0) became evident after three days of dark incubation. This indicates that senescence had been initiated at this

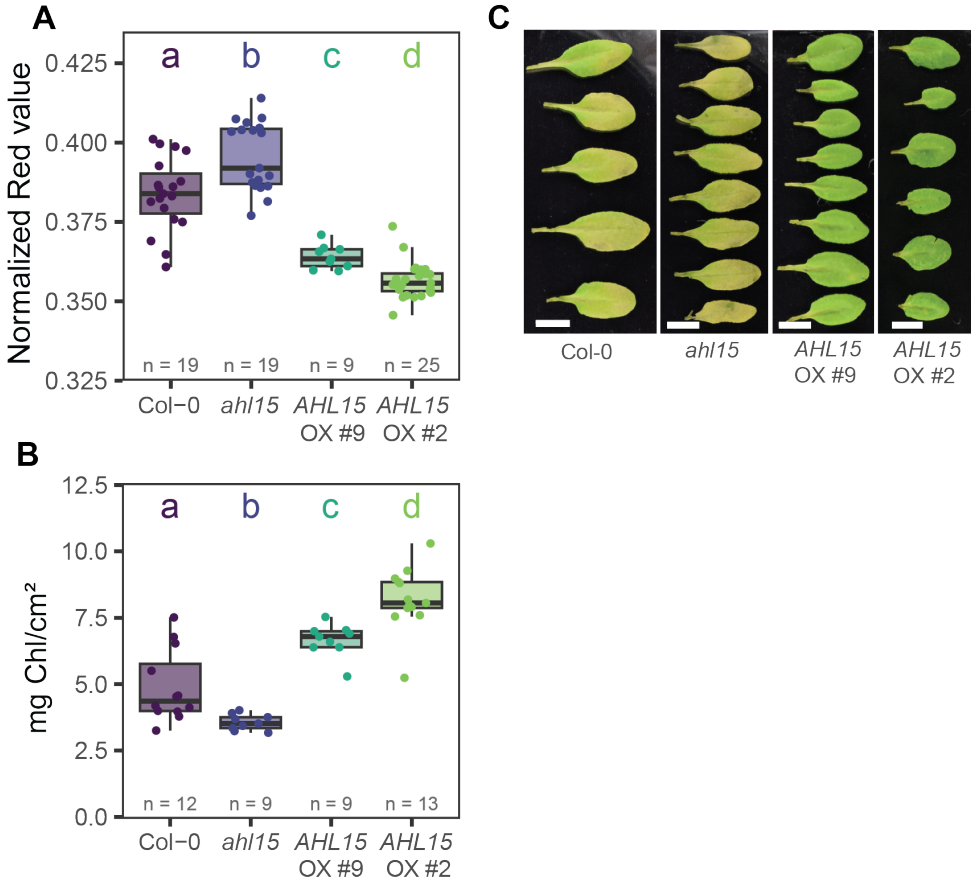

Figure 2: Dark-induced *s*enescence is delayed in leaves detached from *AHL15* OX (*p35S:3x-FLAG-AHL15*) plants and accelerated in ahl15 loss-of-function plants. **A-C**: The fifth leaf of 23 day-old plants was floated on 5 mM MES buffer for five days in the dark to induce the senescence process. Leaves were imaged for chlorophyll quantification as the normalized Red value (Rn) (**A**). Chlorophyll was extracted and quantified by spectrophotometer (**B**). Representative images of leaves of each genotype (**C**). Differences between genotypes in **A** and **B** were compared by a Kruskal-Wallis test, and significance groups are indicated by letters (n=9-25; $p < 0.05$). White bars in **C** represent 1 cm.

time point in non-induced leaves (Figure 3A-C). To determine whether AHL15 inhibits senescence at its onset or at a later stage, we measured the expression of *SENESCENCE-ASSOCIATED GENE (SAG) SAG13* and *SAG12,* which are associated with early- and late senescence, respectively (Lohman et al., 1994). RNA was isolated from leaves right before dark incubation and DEX treatment (day 0), and after three or five days of dark incubation with and without DEX treatment. A clear and significant difference in the expression of the early senescence marker *SAG13* as well as the late senescence marker *SAG12* was visible between DEX- and mock-treated plants (Figure 3D-E), whereas no difference was seen in the expression of *SEN1,* whose expression is induced by darkness (Oh et al., 1996; Chung et al., 1997; Supplementary figure 1). These results indicate that overexpression of *AHL15* affects the onset of senescence at an early stage but does not interfere with the response to darkness.

AHL15 directly represses the expression of *ORESARA1* and several *CKX* genes

ChIP-seq was performed using *AHL15* OX (*p35S:3xFLAG-AHL15*) plants to identify direct targets of AHL15 (this thesis chapter 5). This showed that AHL15 binds up- and downstream of many genes, among which the *SQUAMOSA PROMOTER BINDING PROTEIN-LIKE 9* (*SPL9*) gene, whose expression was previously shown to be suppressed by AHL15 (Rahimi et al., 2022a). Significant peaks were present at 600 bp upstream and 1 kb downstream of the senescence regulator *ORESARA1* (*ORE1*), which could explain the delayed senescence phenotype observed in *AHL15* overexpressing plants (Figure 4A). We next measured the expression of *ORE1* after senescence induction of DEX- or mock-treated leaves and saw that its expression was strongly repressed in DEX-treated leaves, implying a direct repression of this gene by AHL15 (Figure 4B).

In addition, we identified the *CKX* genes *2*, *3*, and *5* (Figure 4A) and several CK biosynthesis genes (*IPT7, LOG1, LOG7, LOG8;* Supplementary figure 2A) among the significant ChIP-seq peaks. Because of the previous finding that AHL15 promotes wood formation by enhancing CK levels (Rahimi et al., 2022b), and because CKs are known to have an inhibitory effect on leaf senescence (Kim et al., 2006; Guo and Gan, 2011; Hu et al., 2021; Yang et al., 2022), we hypothesized that the delayed senescence phenotype of *AHL15* overexpressing plants could in part be a result of increased CK levels. To test whether AHL15 directly regulates the expression of these genes, we measured the expression of each of these genes at 0, 3, or 5 days after senescence induction in DEX- or mock-treated

p35S:AHL15-GR leaves. The expression of *LOG8* and the three *CKX* genes in mock-treated leaves followed a similar pattern as the senescence markers *SAG13* and *SAG12*, and were all increased after 3 and 5 days of dark incubation (Figure 4B, Supplementary figure 2B). In contrast, the expression of *IPT7* and *LOG1* in mock-treated leaves was lower than at day 0, and the expression of *LOG7* was not affected (Supplementary figure 2B). Interestingly, the expression of the *CKX* genes was significantly lower in DEX-treated leaves compared

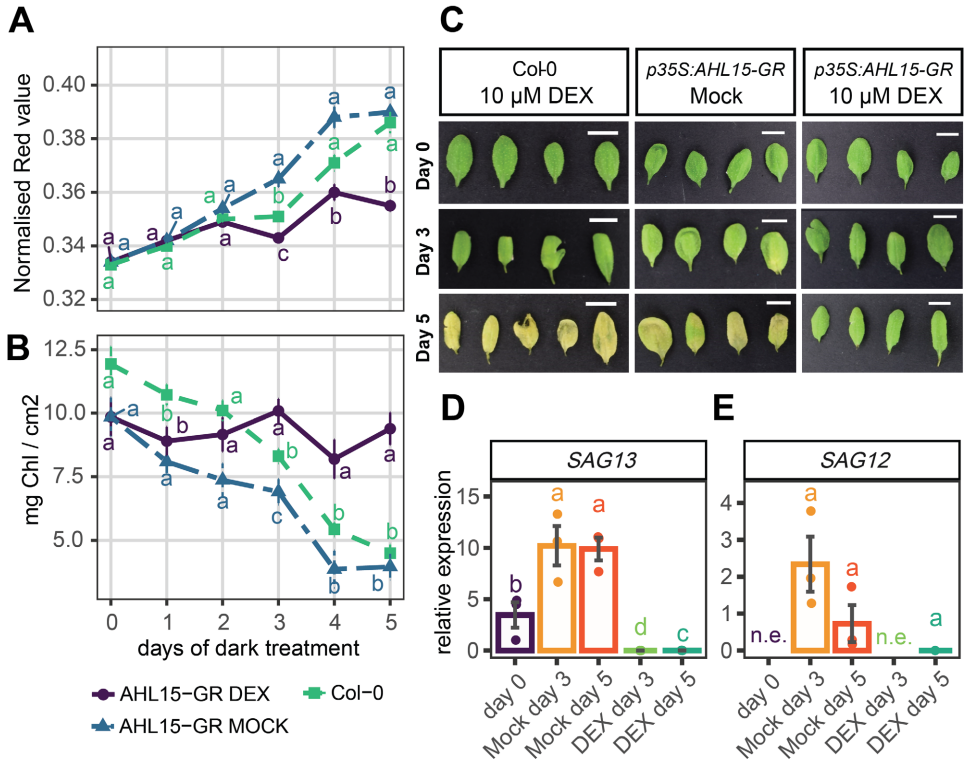

Figure 3: DEX-induced nuclear localization of AHL15-GR inhibits leaf senescence. **A-B**: quantification of chlorophyll in Col-0 and *p35S:AHL15-GR* leaves with and without DEX treatment over five days of dark incubation. The fifth leaf was taken from 23 day-old plants and incubated in the dark on 5 mM MES buffer with or without 10 µM DEX for the indicated number of days. Image-based calculation of the normalized Red value (**A**) or direct chlorophyll extraction (**B**) was used to quantify leaf chlorophyll content of eight leaves per time point (n = 8). **C**: representative images of leaves from each group before and after three or five days of dark incubation. White bars represent 1 cm. **D** and **E**: expression of senescence-associated genes (SAG) in DEX-or Mock-treated leaves. Gene expression was measured by RT-qPCR on RNA extracted from three samples per time point and condition (n=3), with each sample consisting of the fifth leaf of three individual plants. *SAG12* expression could not be detected (n.d.) at day 0 and in DEX-treated leaves at day 3. Expression was normalized to *ACTIN2*. Letters indicate significance groups calculated with the Kruskall-Wallis test ($p < 0.05$).

to the mock treatment, implying that these genes are directly repressed by AHL15 (Figure 4B). The repression of *IPT7* expression upon dark incubation was delayed in DEX-treated leaves, whereas the expression of *LOG1* and *LOG8* was repressed in comparison to mock-treated leaves and *LOG7* expression was unaffected (Supplementary figure 2B). These data suggest that unlike in stem tissue (Rahimi et al., 2022b), AHL15 does not promote CK biosynthesis during leaf senescence, but rather inhibits its degradation by repressing the expression of *CKX* genes.

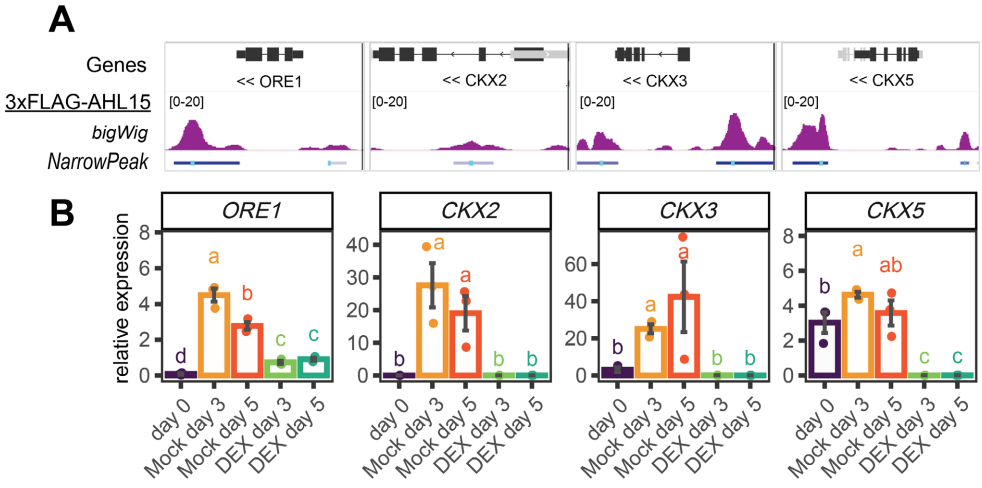

Figure 4: AHL15 directly regulates *ORE1* and *CKX* genes when overexpressed. **A**: ChIP peaks of AHL15 1 kb downstream and 600bp upstream of *ORE1*, in the second intron of *CKX2*, 1.9 kb upstream and directly downstream of *CKX3*, and at 2.3 kb upstream and 2 kb downstream of *CKX5*. ChIP was performed on the whole rosette of 31 days old *AHL15* OX (*p35S:3xFLAG-AHL15*) plants using an anti-flag antibody to pull down AHL15-bound DNA. The figure shows read alignment in purple (bigwig track), and the location of significant peaks in blue (narrowpeak track); a light blue bar indicates the peak summit. Significant peaks can be seen at the loci of *ORE1*, *CKX2, 3*, and *5*. Similar results were obtained in three biological replicates. **B**: The expression of *ORE1*, *CKX2, 3* and *5* is repressed by AHL15 in dark-incubated leaves. Leaves of 23 days old plants were floated on 5 mM MES buffer with or without 10 μM DEX for the indicated number of days in the dark. RNA used for RT-qPCR was extracted from three samples per time point and condition (n=3), with each sample consisting of the fifth leaf of three individual plants. Expression levels are relative to that of *ACTIN2*. Letters indicate significance groups as calculated by the Kruskall-Wallis test ($p < 0.05$).

Cytokinin levels are increased in *AHL15* overexpressing plants

The repression of *CKX* genes by AHL15 suggests that the inactivation of CKs is delayed in *AHL15*-overexpressing leaves, resulting in increased CK levels that repress the onset of senescence. To test whether this was the case, we measured the levels of a wide range of CKs in dark-induced *AHL15-GR* leaves

with and without DEX treatment before and during senescence (Figure 5, Supplementary figures 3-8). These measurements showed that total CK levels drop upon senescence induction in both DEX- and mock-treated leaves but that this decrease in CK levels is less pronounced in DEX-treated leaves (Figure 5A). This trend was especially clear for the isopentenyladenine (iP)-glucosides (Figure 5B, Supplementary figure 4), implying that they may be especially sensitive to degradation by CKX enzymes during the senescence process. Previous research has shown that both iP and iP-9-glucoside (IP9G) , but not iP-7-glucoside (iP7G) can inhibit senescence in Arabidopsis cotyledons (Hallmark and Rashotte, 2020). Although iP in its base form was not present at detectable levels in any of the samples, the elevated levels of iP9G in DEX-treated samples may partially explain the delayed senescence phenotype. In addition, the levels of trans-Zeatin base and trans-Zeatin Riboside (tZ and tZR) were reduced in all dark-incubated samples, but their concentration remained significantly higher in DEX-treated leaves (Figure 5C, D). Of all CK types, tZ-base and tZR have been shown to be among the most potent inhibitors of senescence (Hönig et al., 2018; Pokorná et al., 2020), and their elevated concentration in DEX- versus mock-treated leaves could therefore play an important role in senescence inhibition in DEX-treated leaves.

In addition to tZ and iP, we profiled the levels of cis-zeatine (cZ) and dihydrozeatin (DHZ) during the senescence process (Supplementary figure 6 and 7). Interestingly, cZ-base and cZG levels increased upon dark induction and were especially high after five days of DEX treatment (Supplementary figure 6). cZ has a weak effect on leaf senescence, and its function in the plant remains largely unknown (Gajdošová et al., 2011). Previous research has shown that DHZ levels drop during the senescence process in tobacco leaves (Hönig et al., 2018), and we observed a similar trend in our experiment. While DHZ-base levels were undetectable, we found that DHZ derivatives were present at reduced levels in all samples and that these levels did not differ significantly between treatments, indicating that this form of CK is not affected by AHL15 and its downstream targets (Supplementary figure 7). Finally, we observed an overall increase in CK bases in DEX-treated samples compared to untreated and mock-treated samples (Supplementary figure 3), suggesting that other CK bases may be of importance in the AHL15-mediated delay of senescence.

Taken together, our results indicate that AHL15 can repress senescence in different ways: by directly repressing *ORE1* expression, and by repressing *CKX* expression and thereby delaying inactivation of CKs in leaves. The latter process results in elevated CK levels in *AHL15*-overexpressing leaves,

ultimately contributing to the delay in leaf senescence (Figure 6).

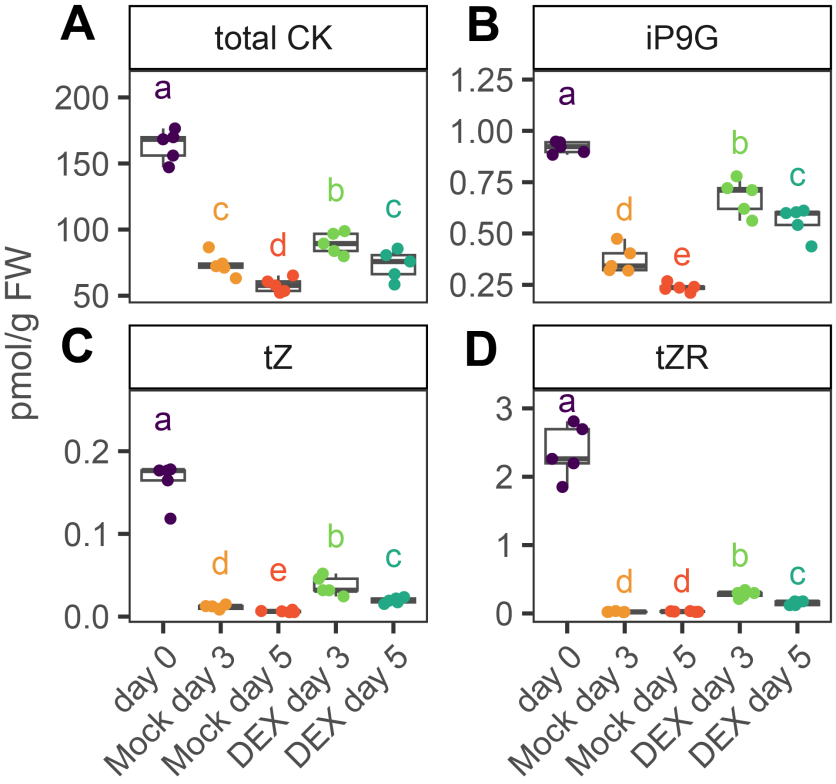

Figure 5: The effect of AHL15 induction on CK levels in dark-incubated leaves. **A**: Total CK; **B**: isopentenyladenine-9-glucoside; **C**: trans-zeatin base; **D**: trans-zeatin riboside. The fifth leaf was collected from 23-day old plants and floated on 5 mM MES with or without 10 µM DEX and stored in the dark for the indicated number of days. Material of three leaves was pooled for each sample, and five samples were measured for each condition (n = 5). Groups were compared using the Kruskall-Wallis test, and letters indicate significance groups ($p < 0.05$).

Discussion

AHL15 has previously been shown to delay several developmental processes, including vegetative phase change, flowering time, and axillary meristem maturation (Karami et al., 2020; Rahimi et al., 2022a). Our data show that in addition to these processes, AHL15 delays leaf senescence by directly repressing expression of *ORE1* encoding a key senescence regulator and by inhibiting CK degradation by repressing *CKX* expression. These two processes are likely to act in parallel and together explain the strong stay-green phenotype observed in *AHL15* overexpressing plants (Figure 6). Moreover, our data suggest that

AHL15 acts predominantly by repressing gene expression, as was the case for *ORE1* and three *CKX* genes.

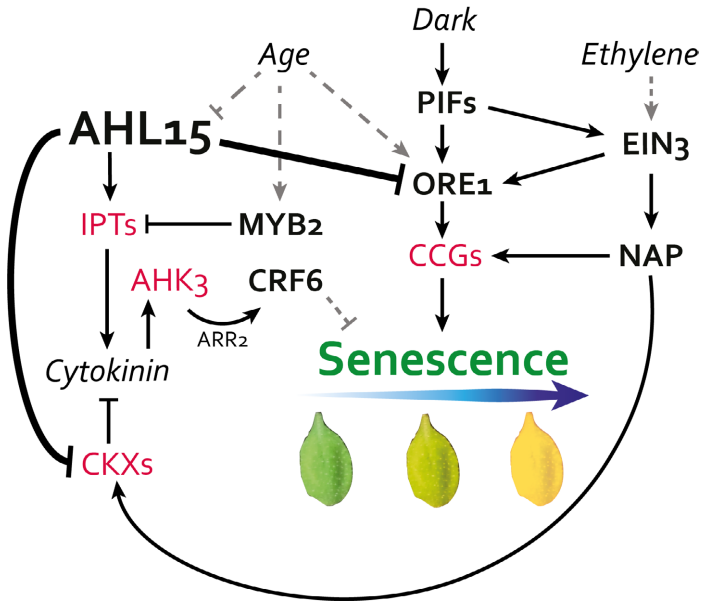

Figure 6: Model of AHL15-mediated repression of senescence. AHL15 represses ORESARA1 (ORE1), which is an important positive regulator of senescence. ORE1 can be induced by dark incubation via the PHYTOCHROME INTERACTING FACTORS (PIFs), by ethylene via ETHYLENE INSENSITIVE 3 (EIN3), or by age. ORE1 activates many downstream targets among which chlorophyll catabolic genes (CCGs) that ultimately lead to chlorophyll catabolism that causes the characteristic yellowing of senescent leaves. NAC-LIKE, ACTIVATED BY AP3/PI (NAP) acts in parallel to ORE1 and activates expression of CCGs as well as the CYTOKININ OXIDASE/DEHYDROGENASE (CKX) genes which can irreversibly inactivate cytokinins (CKs). CKs inhibit leaf senescence via ARABIDOPSIS HISTIDINE KINASE 3 (AHK3), which represses leaf senescence via CYTOKININ RESPONSE FACTOR 6 (CRF6). CKs are produced by ISOPENTENYL TRANSFERASE (IPT) enzymes, which are transcriptionally repressed by MYB2 in ageing plants. AHL15 represses *CKX* expression, and promotes expression of *IPT7*. Lower CKX levels result in slower breakdown of CKs, resulting in higher CK levels and delayed senescence. TFs are indicated with bold letters, enzymes are indicated in red, and hormones and external abiotic factors are written in italics.

ORE1 acts as a key transcriptional regulator of senescence, and its expression is induced by several senescence-promoting environmental cues. Ethylene promotes the expression of *ORE1* and *NAP* via EIN3 (Li et al., 2013; Kim et al., 2014), ABA promotes *ORE1* expression via the TF ACTIVATING FACTOR1 (ATAF1) (Garapati et al., 2015), and dark incubation leads to enhanced *ORE1* transcription via the PIF TFs (Song et al., 2014). It was also shown that *ORE1* expression is post-transcriptionally silenced in young leaves by miR164, and that this silencing is relieved with progressing age (Kim et al., 2009; Li et al.,

2013). Here, we have identified AHL15 as a novel repressor of *ORE1* expression, suggesting that AHL15 can antagonize the ethylene- and dark-induced senescence processes mediated by ORE1. In addition, *AHL15* is strongly expressed in juvenile plants and developing leaves, and is gradually silenced over developmental age (Rahimi et al., 2022a). It is therefore possible that AHL15 can act as an additional age-dependent repressor of *ORE1* expression in parallel to miR164 (Figure 6).

CK has long been known to inhibit leaf senescence, but relatively little is known about its position in the senescence pathway. Application or overproduction of CK can block the onset of leaf senescence (Richmond et al., 1957; Gan and Amasino, 1995; Kim et al., 2006; Argueso and Kieber, 2024), and it has been shown that CK degradation is promoted during the senescence process by NAP-mediated upregulation of *CKX* expression (Hu et al., 2021; Li et al., 2023). MYB2 was shown to lower CK production in an age-dependent manner by repressing the expression of several *IPT* genes, which are the rate-limiting enzymes in the CK biosynthesis pathway (Guo and Gan, 2011). Our data show that AHL15 acts antagonistically to NAP in *CKX* transcriptional regulation, and represses senescence via inhibition of CK degradation. In addition, we found that *IPT7* expression decreased in response to dark-induced senescence, and that this process was delayed after activation of AHL15-GR by DEX treatment. Taken together, our results indicate that AHL15 acts as a positive regulator of CK in the senescence pathway, and thereby acts antagonistically to NAP and MYB2 in this process (Figure 6).

Our experiments show that the expression of the CK biosynthesis genes *LOG1* and *IPT7* is downregulated upon senescence induction by dark treatment. On the other hand, we observed an increased expression of *LOG8* after senescence induction, and that *LOG7* expression is stable throughout the senescence process. In addition, the levels of cZ in its base form and most of its derivatives were increased in senescent leaves. Together, these data show that CK biosynthesis is not completely repressed but partially maintained during the senescence developmental program. Our data also confirm the previously reported induction of *CKX* expression during senescence. This indicates that CK levels are regulated both by biosynthesis and by degradation during the senescence process, and suggests a role for some CK variants in the senescence process. Finally, our data show that inhibition of CK breakdown by direct silencing of *CKX* genes partially explains the delayed senescence phenotype of *AHL15* overexpressing plants. Previously, it was shown that expression of *LOG4*, *IPT3* and *IPT7* was decreased in *ahl15* knockout plants, resulting in lower

CK levels and a decrease in radial xylem width (Rahimi et al., 2022b). Here, we observed delayed downregulation of *IPT7* in dark-incubated leaves following DEX-induced nuclear localization of AHL15-GR, indicating that AHL15 targets are partially shared between stem and leaf tissue.

Our data show that the senescence phenotype of *ahl15* leaves is relatively mild. This suggests that AHL15 plays a minor role in senescence in wild-type plants, or that its function is compensated for by other AHLs when it is absent in *ahl15* knockout plants. *AHL* genes have been shown to be highly functionally redundant, and developmental phenotypes are observed only in higher-order *ahl* mutants (Xiao et al., 2009; Zhao et al., 2013; Karami et al., 2020; Rahimi et al., 2022a). It is therefore possible that higher-order *ahl* mutants show a more clear acceleration of leaf senescence than the *ahl15* single mutant, and that knockout of clade-A *ahl* genes that are expressed in adult leaves will have a more pronounced phenotype. In addition, *AHL15* is expressed primarily in juvenile tissues of wild-type plants, and no GUS activity was seen in expanded or adult leaves when expressed under the *AHL15* promoter (Rahimi et al., 2022a). It is therefore likely that leaves of *ahl15* and wild-type plants do not significantly differ from each other because *AHL15* is not expressed in fully grown wild-type leaves, explaining the similarity in senescence phenotype between the two genotypes.

The functional redundancy between AHL proteins also implies that overexpression of other clade-A *AHLs* could have similar effects as AHL15 on the expression of *ORE1* and *CKX* genes and the overall CK levels in the plant, and that the repression of CK degradation is a general effect of high AHL dosage. Overexpression of at least one other clade-A *AHL, AHL27,* has been shown to inhibit senescence (Lim et al., 2007b), indicating that like flowering time, the senescence-inhibiting phenotype could be induced by multiple AHLs in this clade. It would therefore be interesting to see whether overexpression of other clade-A *AHLs* has a similar senescence phenotype as *AHL15* and *AHL27*, and whether this coincides with a higher CK level in the leaves. Arabidopsis contains 15 clade A *AHLs*, and the genomes of most crop species contain a similar or higher number of *AHL* genes (Zhao et al., 2014; Zhao et al., 2020; Machaj and Grzebelus, 2021; Zhang et al., 2021b; Wang et al., 2023). Breeding efforts to improve longevity and shelf life could focus on enhancing expression of clade-A *AHLs,* which, due to their functional overlap and large number, could provide convenient breeding targets.

Methods

Plant material and growth conditions

Seeds were sown on damp soil (90% turf soil with 10% sand) and stratified for three days at 4 °C before transfer to a climate chamber set at 21°C with long day (16h photoperiod) and 65% relative humidity. Seedlings were transferred to individual pots at one week after sowing and plants were watered weekly.
The *p35S:AHL15-GR* overexpression and *ahl15* loss-of-function lines were described previously (Karami et al., 2020). *p35S:3xFLAG-AHL15* overexpression lines were generated by replacing the *AHL15-GR* construct in the *p35S:AHL15-GR* vector made by Karami et al. (2020) with a synthetic *3xFLAG-AHL15* construct, which was transformed to *Agrobacterium tumefaciens* strain AGL1 by electroporation (Dulk-Ras and Hooykaas, 1995). Transgenic *p35S:AHL15* Arabidopsis Col-0 lines were obtained by the floral dip method (Clough and Bent, 1998) and by subsequently selecting T1 and T2 plants on ½ MS medium supplemented with 15 mg/L phosphinotricin. Single locus transgenic lines, showing a 3:1 segregation ratio of resistant : susceptible plants in the T2 generation, were selected and T3 seeds from homozygous T2 plants were subsequently used for senescence experiments.

For dark-induced senescence assays, fifth leaves were detached from the plants at 23 days after the start of germination and floated on 5 mM MES buffer (pH 5.6) in 5 cm ø Petri dishes, with a maximum of 10 leaves per dish. Petri dishes were sealed with parafilm, wrapped in aluminium foil, and stored in a cardboard box which was placed in the growth chamber to ensure a constant temperature at 20 °C. For the hormone treatments, a 10 mM dexamethasone (ThermoFisher, Vilnius, Lithuania) stock solution dissolved in DMSO was diluted 1000-fold in 5 mM MES buffer. For mock treatment, DMSO was diluted 1000-fold in 5 mM MES buffer.

Senescence measurements

For colorimetric measurements, the leaves were imaged on a dark background with a white reference card under uniform lighting with a Nikon DC3000 camera, with the following settings: ISO 160, exposure time 1/160 s. Image analysis was done in ImageJ with a self-made plugin (this thesis chapter 3). The analysis consisted of the following steps: white balancing of images based on a white reference sheet included in each picture; removal of background, conversion to an RGB image stack, automatic selection of individual leaves,

and measurement of pixel intensity for each leaf in each of the red, green, and blue channels. The mean red, green, and blue values for each leaf were used to calculate the Green: Red ratio and the normalized red value (Rn; Red/(Red+Green+Blue)).

After imaging for colorimetric measurements, two 5 mm ø leaf disks were taken from each leaf and stored at -80 °C. Aceton extraction was done following the method described by Arnon (1949). Briefly, frozen leaf material was pulverized with a metal bead and dissolved in 200 µL 25 mM sodium phosphate buffer (pH 7) and 800 µL 80% acetone. Samples were then incubated at room temperature for 1 hour with gentle shaking, and centrifuged for 10 minutes at 2500x*g*. 200 µL supernatant was then transferred to a clear-bottomed 96-well plate and the absorption (D) at 645 and 663 nm was measured with a TECAN Spark plate reader (Männedorf, Switzerland). The total chlorophyll content in mg/L was then calculated with the following formula: $Chl_{Total} = 20{,}2*D_{645} + 8{,}02*D_{663}$, as described by (Arnon, 1949), and then corrected for the total area of leaf tissue used for Chl extraction. Spectrophotometry results and colorimetric results from ImageJ were processed in R (R Core Team, 2023). Plots were generated using ggplot2 (Wickham, 2016) and ggpubr (Kassambara, 2023), and genotypes or treatments were compared with the Kruskal-Wallis test by using the package Agricolae (de Mendiburu, 2023).

RNA isolation and RT-qPCR

After imaging for colorimetric measurements, leaves were cut in half, of which one half was used for RNA extraction, while the other half of each leaf was used for chlorophyll extraction. For each RNA extraction, material of three plants was pooled and snap-frozen in liquid nitrogen, and tissue was pulverized with a metal bead using the Qiagen Tissuelyser. RNA was isolated with Trizol© reagent (ThermoFisher, Vilnius, Lithuania) by following the standard protocol for Trizol-based RNA extraction, with an additional ethanol wash step at the RNA precipitation stage. Next, 1 µg of RNA was aliquoted to a new tube and treated with DNAse I (ThermoFisher, Vilnius, Lithuania) at 37 °C for 30 minutes and used for cDNA synthesis with the RevertAid First Strand Kit (ThermoFisher, Vilnius, Lithuania) according to the kit's instructions. RT-qPCR was performed with TB green ex-Taq II (Takara Bio Europe, Saint-Germain-en-Laye, France) on the Quantstudio 5 Real-Time PCR machine (Applied Biosystems, Foster City, USA) in a reaction volume of 5 µL. Primers used for RT-qPCR can be found in Supplementary Table 1 and were synthesized by Sigma Aldrich (Haverhill, UK). Gene expression was normalized to *ACTIN2* expression by using the 2^-ΔΔCT

method (Livak and Schmittgen, 2001), and groups were compared with the Kruskall-Wallis test in R as described above.

Chromatin Immunoprecipitation

The ChIP protocol used here was adapted from the protocols by Kaufmann et al. (2010) and Chouaref et al. (2018). For each ChIP, 1 g shoot tissue of 31 day-old *p35S:3xFLAG-AHL15* plants was harvested and fixated for 10 minutes on ice and under vacuum in 1% formaldehyde in ice-cold MC buffer (10 mM sodium phosphate buffer pH 7, 50 mM NaCl, 0.1 M sucrose). The fixation reaction was stopped by addition of glycine to a concentration of 114 mM. Next, samples were washed with ice-cold MC buffer, dried thoroughly, flash-frozen and stored at -80 °C. For nuclei isolation, fixated tissue was ground to a very fine powder in liquid nitrogen using a mortar and pestle and resuspended in 15 mL M1 buffer (10 mM sodium phosphate buffer pH 7, 0.1 M NaCl, 1 M 2-methyl 2,4-pentanediol, 10 mM β-mercaptoethanol) in a 50 mL tube, which was gently shaken at 4 °C for 30 minutes. Suspensions were successively filtered through a 100 µM and 70 µM nylon mesh, both of which were washed with an additional 5 mL M1 buffer to extract additional nuclei. The filtered suspension was then centrifuged for 20 minutes at 1000x*g* at 4°C, and pellets were resuspended in 20 mL M2 buffer (10 mM sodium phosphate buffer pH 7, 0.1 M NaCl, 1 M 2-methyl 2,4-pentanediol, 10 mM β-mercaptoethanol, 10 mM $MgCl_2$, 0.5% Triton X-100). After 30 minutes of gentle shaking at 4 °C, the suspension was centrifuged for 10 minutes at 1000x*g* at 4 °C, the supernatant was discarded, and the pellet was resuspended again in 5 mL M2 buffer. After 10 minutes of gentle shaking followed by 10 minutes centrifugation at 1000x*g* at 4 °C, the pellet was resuspended in 1 mL sonication buffer (10 mM sodium phosphate buffer pH 7, 0.1 M NaCl, 0.5% Sarkosyl, 10 mM EDTA) and aliquoted to 300 µL in 1.5 mL protein lobind tubes (Eppendorf, Germany). Samples were then sonicated for 5 rounds of 10 cycles of 30 seconds ON / 30 seconds OFF on HIGH in a Bioruptor sonicator (Diagenode, Serain, Belgium) to a fragment size of ~300 bp. After sonication, tubes of the same replicate were pooled and centrifuged for 10 minutes at 12000x*g* at 4 °C, and supernatant was transferred to a new protein lobind tube and stored at -20 °C overnight.

For the immunoprecipitation, 50 µg chromatin was used per IP (ca 250 µL sonicated material), and 3.5 volumes IP buffer (50mM HEPES pH7.5, 150 mM NaCl, 5 mM $MgCl_2$, 10 µM $ZnSO_4$, 1% Triton X-100, 0.05% SDS) and 25 µL protein G dynabeads (ThermoFischer, Vilnius, Lithuania) conjugated to mouse monoclonal Anti-FLAG M2 antibodies (F1804; Sigma-Aldrich, Darmstadt,

Germany) were added and rotated at 4 °C overnight. After this, beads were washed once in 1 mL each of the following buffers: IP buffer, high salt buffer (500 mM NaCl, 0.1% SDS, 1% Triton X-100, 2 mM EDTA, 20 mM Tris-HCl pH 8), LiCl buffer (10 mM Tris-HCl pH 8, 1 mM EDTA, 1% NP-40, 1% sodium deoxycholate, 0.25 M LiCl), and twice in TE buffer (10 mM Tris-HCl pH 8, 1 mM EDTA), and then resuspended in 50 µL TE buffer. Samples were decrosslinked overnight at 65 °C in nine volumes of decrosslinking buffer (50 mM Tris-HCl pH 8, 10 mM EDTA pH 8, 250 mM NaCl, 1 % (w/v) SDS). DNA was isolated with the phenol : chloroform method, resuspended in water and treated with RNAse A (ThermoFischer, Vilnius, Lithuania) for 30 minutes at 37 °C, and then stored at -20 °C until further use.

ChIPped DNA was sequenced at Macrogen (Amsterdam, NL) with 20M 150 bp paired-end reads. ChIP-seq analysis was done using the nextflow ChIP-seq pipeline (Ewels et al., 2020), and the TAIR10 version of the Arabidopsis genome was used for read mapping. Reads were annotated in R using the ChIPSeeker package (Yu et al., 2015; Wang et al., 2022).

Cytokinin measurements

Quantification of cytokinin metabolites was performed on biological replicates according to the method described by Svağinová et al. (2012) including modifications described by Antoniadi et al. (2015). Samples (10 mg fresh weight) were homogenized and extracted in 1 ml of modified Bieleski buffer (60% methanol, 10% formic acid and 30% water) together with a cocktail of stable isotope-labeled internal standards (0.2 pmol of CK bases, ribosides, N-glucosides, and 0.5 pmol of CK O-glucosides, nucleotides per sample added). The extracts were applied onto an Oasis MCX column (30 mg/1 ml, Waters) conditioned with 1 ml each of 100% methanol and water, equilibrated sequentially with 1ml of 50% (v/v) nitric acid, 1 ml of water, and 1 ml of 1M formic acid, and washed with 1 ml of 1M formic acid and 1 ml 100% methanol. Analytes were then eluted by two-step elution using 1 ml of 0.35M ammonium hydroxide aqueous solution and 2 ml of 0.35M NH4OH in 60% (v/v) MeOH solution. The eluates were then evaporated to dryness in vacuo and stored at -20°C. Cytokinin levels were determined by an ultra-high performance liquid chromatography-electrospray tandem mass spectrometry (UHPLC-MS/MS) using stable isotope-labelled internal standards as a reference (Rittenberg and Foster, 1940). Separation was performed on an Acquity UPLC® i-Class System (Waters, Milford, MA, USA) equipped with an Acquity UPLC BEH Shield RP18 column (150x2.1 mm, 1.7 µm; Waters), and the effluent was introduced into the

electrospray ion source of a triple quadrupole mass spectrometer Xevo™ TQ-S MS (Waters). Five independent biological replicates each consisting of material from the fifth leaf of three plants were performed, including two technical replicates of each.

Acknowledgements

We thank Jan Vink, Altay Temel, Ward de Winter and Mariel Lavrijsen for technical support and Marion Larue and Jelmer van Lieshout for help with setting up the project. This work was supported the graduate school green top sectors grant (grant nr. GSGT.2019.024) from the Dutch Research Council (NWO) to TL.

Literature

Antoniadi I., Placková L., Simonovik B., Doležal K., Turnbull C., Ljung K., Novák O. (2015). Cell-type-specific cytokinin distribution within the Arabidopsis primary root apex. Plant Cell **27**: 1955–1967.

Argueso C.T., Kieber J.J. (2024). Cytokinin: From autoclaved DNA to two-component signaling. Plant Cell 1–22.

Balanzà V., Martínez-Fernández I., Sato S., Yanofsky M.F., Kaufmann K., Angenent G.C., Bemer M., Ferrándiz C. (2018). Genetic control of meristem arrest and life span in Arabidopsis by a FRUITFULL-APETALA2 pathway. Nat Commun **9**: 565.

Balazadeh S., Siddiqui H., Allu A.D., Matallana-Ramirez L.P., Caldana C., Mehrnia M., Zanor M.I., Köhler B., Mueller-Roeber B. (2010). A gene regulatory network controlled by the NAC transcription factor ANAC092/AtNAC2/ORE1 during salt-promoted senescence. Plant J **62**: 250–264.

Chouaref J., de Boer E., Fransz P., Stam M. (2018). Protocol for Chromatin Immunoprecipitation of meiotic-stage-specific tomato anthers. Curr Protoc Plant Biol **3**: e20074.

Chung B.-C., Lee S.Y., Oh S.A., Rhew T.H., Nam H.G., Lee C.-H. (1997). The promoter activity of *sen1*, a senescence-associated gene of Arabidopsis, is repressed by sugars. J Plant Phys **151**: 339–345.

Clough S.J., Bent A.F. (1998). Floral dip: a simplified method for *Agrobacterium*-mediated transformation of *Arabidopsis thaliana*. Plant J **16**: 735–743.

Dulk-Ras A. den, Hooykaas P.J.J. (1995). Electroporation of *Agrobacterium tumefaciens*. Plant Cell Electroporation And Electrofusion Protocols. Humana Press, New Jersey, pp 63–72

Ewels P.A., Peltzer A., Fillinger S., Patel H., Alneberg J., Wilm A., Garcia M.U., Di Tommaso P., Nahnsen S. (2020). The nf-core framework for community-curated bioinformatics pipelines. Nat Biotech **38**: 276–278.

Gajdošová S., Spíchal L., Kamínek M., Hoyerová K., Novák O., Dobrev P.I., Galuszka P., Klíma P., Gaudinová A., Žižková E., et al (2011). Distribution, biological activities, metabolism, and the conceivable function of cis-zeatin-type cytokinins in plants. J EXP BOT **62**: 2827–2840.

Galuszka P., Frébort I., Šebela M., Pec P. (2000). Degradation of cytokinins by cytokinin oxidases in plants. Plant Growth Regul **32**: 315–327.

Gan S., Amasino R.M. (1995). Inhibition of leaf senescence by autoregulated production of cytokinin. Science (1979) **270**: 1986–1988.

Garapati P., Xue G.P., Munné-Bosch S., Balazadeh S. (2015). Transcription factor ATAF1 in Arabidopsis promotes senescence by direct regulation of key chloroplast maintenance and senescence transcriptional cascades. Plant Physiol **168**: 1122–1139.

Guo Y., Gan S. (2006). AtNAP, a NAC family transcription factor, has an important role

in leaf senescence. Plant J **46**: 601–612.

Guo Y., Gan S. (2011). *AtMYB2* regulates whole plant senescence by inhibiting cytokinin-mediated branching at late stages of development in Arabidopsis. Plant Physiol **156**: 1612–1619.

Guo Y., Ren G., Zhang K., Li Z., Miao Y., Guo H. (2021). Leaf senescence: progression, regulation, and application. Mol Hortic **1**: 1–25.

Hallmark H.T., Rashotte A.M. (2020). Cytokinin isopentenyladenine and its glucoside isopentenyladenine-9G delay leaf senescence through activation of cytokinin-associated genes. Plant Direct **4**: e00292.

Hönig M., Plíhalová L., Husicková A., Nisler J., Doležal K. (2018). Role of cytokinins in senescence, antioxidant defence and photosynthesis. Int J Mol Sci. doi: 10.3390/IJMS19124045

Hu Y., Liu B., Ren H., Chen L., Watkins C.B., Gan S.S. (2021). The leaf senescence-promoting transcription factor AtNAP activates its direct target gene *CYTOKININ OXIDASE 3* to facilitate senescence processes by degrading cytokinins. Mol Hortic **1**: 1–12.

Jordi W., Schapendonk A., Davelaar E., Stoopen G.M., Pot C.S., De Visser R., Van Rhijn J.A., Gan S., Amasino R.M. (2000). Increased cytokinin levels in transgenic *PSAG12–IPT* tobacco plants have large direct and indirect effects on leaf senescence, photosynthesis and N partitioning. Plant Cell Environ **23**: 279–289.

Kakimoto T. (2001). Identification of plant cytokinin biosynthetic enzymes as dimethylallyl diphosphate: ATP/ADP isopentenyltransferases. Plant Cell Phys **42**: 677–685.

Karami O., Rahimi A., Khan M., Bemer M., Hazarika R.R., Mak P., Compier M., van Noort V., Offringa R. (2020). A suppressor of axillary meristem maturation promotes longevity in flowering plants. Nat Plants **6**: 368–376.

Kassambara A. (2023). ggpubr: "ggplot2" Based Publication Ready Plots.

Kaufmann K., Muiño J.M., Østerås M., Farinelli L., Krajewski P., Angenent G.C. (2010). Chromatin immunoprecipitation (ChIP) of plant transcription factors followed by sequencing (ChIP-SEQ) or hybridization to whole genome arrays (ChIP-CHIP). Nat Protoc **5**: 457–472.

Kim H.J., Hong S.H., Kim Y.W., Lee I.H., Jun J.H., Phee B.K., Rupak T., Jeong H., Lee Y., Hong B.S., et al (2014). Gene regulatory cascade of senescence-associated NAC transcription factors activated by ETHYLENE-INSENSITIVE2-mediated leaf senescence signalling in Arabidopsis. J EXP BOT **65**: 4023–4036.

Kim H.J., Ryu H., Hong S.H., Woo H.R., Lim P.O., Lee I.C., Sheen J., Nam H.G., Hwang I. (2006). Cytokinin-mediated control of leaf longevity by AHK3 through phosphorylation of ARR2 in Arabidopsis. PNAS **103**: 814–819.

Kim J.H., Woo H.R., Kim J., Lim P.O., Lee In Chul, Choi S.H., Hwang D., Hong G.N. (2009). Trifurcate feed-forward regulation of age-dependent cell death

involving miR164 in Arabidopsis. Science (1979) **323**: 1053–1057.

Kuroha T., Tokunaga H., Kojima M., Ueda N., Ishida T., Nagawa S., Fukuda H., Sugimoto K., Sakakibara H. (2009). Functional analyses of LONELY GUY cytokinin-activating enzymes reveal the importance of the direct activation pathway in Arabidopsis. Plant Cell **21**: 3152–3169.

Li F., Shan Y., Wang H., Jiang G., Ding X., Liang H., Wang C., Kong X., Xie L., Jiang Y. (2023). A NAC transcriptional factor BrNAC029 is involved in cytokinin-delayed leaf senescence in postharvest Chinese flowering cabbage. Food Chem **404**: 134657.

Li Z., Peng J., Wen X., Guo H. (2013). *ETHYLENE-INSENSITIVE3* is a senescence-associated gene that accelerates age-dependent leaf aenescence by directly repressing *miR164* transcription in Arabidopsis. Plant Cell **25**: 3311.

Lim P.O., Kim H.J., Nam H.G. (2007a). Leaf Senescence. Annu Rev Plant Biol **58**: 115–136.

Lim P.O., Kim Y., Breeze E., Koo J.C., Woo H.R., Ryu J.S., Park D.H., Beynon J., Tabrett A., Buchanan-Wollaston V., et al (2007b). Overexpression of a chromatin architecture-controlling AT-hook protein extends leaf longevity and increases the post-harvest storage life of plants. Plant J **52**: 1140–1153.

Livak K.J., Schmittgen T.D. (2001). Analysis of Relative Gene Expression Data Using Real-Time Quantitative PCR and the 2^-ΔΔCT Method. Methods **25**: 402–408.

Lohman K.N., Gan S., John M.C., Amasino R.M. (1994). Molecular analysis of natural leaf senescence in *Arabidopsis thaliana*. Physiol Plant **92**: 322–328.

Machaj G., Grzebelus D. (2021). Characteristics of the *AT-hook motif containing nuclear localized (AHL)* genes in carrot provides insight into their role in plant growth and storage root development. Genes (Basel) **12**: 764.

McCabe M.S., Garratt L.C., Schepers F., Jordi W.J.R.M., Stoopen G.M., Davelaar E., Van Rhijn J.H.A., Power J.B., Davey M.R. (2001). Effects of PSAG12-IPT gene expression on development and senescence in transgenic lettuce. Plant Physiol **127**: 505–516.

de Mendiburu F. (2023). agricolae: Statistical Procedures for Agricultural Research.

Oh S.A., Lee S.Y., Chung I.K., Lee C.-H., Nam H.G. (1996). A senescence-associated gene of *Arabidopsis thaliana* is distinctively regulated during natural and artificially induced leaf senescence. Plant Mol Biol **30**: 739–754.

Pokorná E., Hluska T., Galuszka P., Hallmark H.T., Dobrev P.I., Drábková L.Z., Filipi T., Holubová K., Plíhal O., Rashotte A.M., et al (2021). Cytokinin N-glucosides: occurrence, metabolism and biological activities in plants. Biomolecules **11**: 24.

Qiu K., Li Z., Yang Z., Chen J., Wu S., Zhu X., Gao S., Gao J., Ren G., Kuai B., et al (2015). EIN3 and ORE1 accelerate degreening during ethylene-mediated leaf senescence by directly activating chlorophyll catabolic genes in Arabidopsis. PLoS Genet **11**: e1005399.

R Core Team (2023). R: A Language and Environment for Statistical Computing.

Rahimi A., Karami O., Balazadeh S., Offringa R. (2022a). miR156 -independent repression of the ageing pathway by longevity-promoting AHL proteins in Arabidopsis. New Phytol **235**: 2424–2438.

Rahimi A., Karami O., Lestari A.D., de Werk T., Amakorová P., Shi D., Novák O., Greb T., Offringa R. (2022b). Control of cambium initiation and activity in Arabidopsis by the transcriptional regulator AHL15. Curr Biol **32**: 1764–1775.

Richmond A.E., Lang A., Okumura F.S., Mag B. (1957). Effect of kinetin on protein content and survival of detached *Xanthium* leaves. Science (1979) **125**: 650–651.

Rittenberg D., Foster G.L. (1940). A NEW PROCEDURE FOR QUANTITATIVE ANALYSIS BY ISOTOPE DILUTION, WITH APPLICATION TO THE DETERMINATION OF AMINO ACIDS AND FATTY ACIDS. J Biol Chem **133**: 737–744.

Schippers J.H.M., Schmidt R., Wagstaff C., Jing H.C. (2015). Living to die and dying to live: The survival strategy behind leaf senescence. Plant Physiol **169**: 914–930.

Schmülling T., Werner T., Riefler M., Krupková E., Bartrina y Manns I. (2003). Structure and function of cytokinin oxidase/dehydrogenase genes of maize, rice, Arabidopsis and other species. J Plant Res **116**: 241–252.

Song Y., Yang C., Gao S., Zhang W., Li L., Kuai B. (2014). Age-triggered and dark-induced leaf senescence require the bHLH transcription factors PIF3, 4, and 5. Mol Plant **7**: 1776–1787.

Svacinová J., Novák O., Placková L., Lenobel R., Holík J., Strnad M., Doležal K. (2012). A new approach for cytokinin isolation from Arabidopsis tissues using miniaturized purification: pipette tip solid-phase extraction. doi: 10.1186/1746-4811-8-17

Takei K., Sakakibara H., Sugiyama T. (2001). Identification of genes encoding adenylateisopentenyltransferase, a cytokinin biosynthesis enzyme, in *Arabidopsis thaliana*. J Biol Chem **276**: 26405–26410.

Thomas H. (2013). Senescence, ageing and death of the whole plant. New Phytol **197**: 696–711.

Tokunaga H., Kojima M., Kuroha T., Ishida T., Sugimoto K., Kiba T., Sakakibara H. (2012). Arabidopsis *lonely guy (LOG)* multiple mutants reveal a central role of the LOG-dependent pathway in cytokinin activation. Plant J **69**: 355–365.

Wang L., Li T., Liu N., Liu X. (2023). Identification of tomato *AHL* gene families and functional analysis their roles in fruit development and abiotic stress response. Plant Physiol Biochem **202**: 107931.

Wang Q., Li M., Wu T., Zhan L., Li L., Chen M., Xie W., Xie Z., Hu E., Xu S., et al (2022). Exploring Epigenomic Datasets by ChIPseeker. Curr protoc **2**: e585.

Wickham H. (2016). ggplot2: Elegant Graphics for Data Analysis.

Woo H.R., Kim H.J., Lim P.O., Nam H.G. (2019). Leaf Senescence: Systems and

dynamics aspects. Annu Rev Plant Biol **70**: 347–376.

Xiao C., Chen F., Yu X., Lin C., Fu Y.F. (2009). Over-expression of an AT-hook gene, *AHL22*, delays flowering and inhibits the elongation of the hypocotyl in *Arabidopsis thaliana*. Plant Mol Biol **71**: 39–50.

Yang J., Worley E., Udvardi M. (2015). A NAP-AAO3 tegulatory module promotes chlorophyll degradation via ABA biosynthesis in Arabidopsis leaves. Plant Cell **26**: 4862–4874.

Yang T., Zhang M., Yang Q., Liu K., Cui J., Chen J., Ren Y., Shao Y., Wang R., Li G. (2022). The S40 family members delay leaf senescence by promoting cytokinin synthesis. Plant Physiol Biochem **191**: 99–109.

Yu G., Wang L.G., He Q.Y. (2015). ChIPseeker: an R/Bioconductor package for ChIP peak annotation, comparison and visualization. Bioinformatics **31**: 2382–2383.

Yun J., Kim Y.-S., Jung J.-H., Seo P.J., Park C.-M. (2012). The AT-hook motif-containing protein AHL22 regulates flowering initiation by modifying *FLOWERING LOCUS T* chromatin in Arabidopsis. J Biol Chem **287**: 15307–15316.

Zhang W., Peng K., Cui F., Wang D., Zhao J., Zhang Y., Yu N., Wang Y., Zeng D., Wang Y., et al (2021a). Cytokinin oxidase/dehydrogenase OsCKX11 coordinates source and sink relationship in rice by simultaneous regulation of leaf senescence and grain number. Plant Biotechnol J **19**: 335–350.

Zhang W.M., Fang D., Cheng X.Z., Cao J., Tan X.L. (2021b). Insights into the molecular evolution of *AT-Hook Motif nuclear Localization* genes in *Brassica napus*. Front Plant Sci. doi: 10.3389/fpls.2021.714305

Zhao J., Favero D.S., Peng H., Neff M.M. (2013). *Arabidopsis thaliana AHL* family modulates hypocotyl growth redundantly by interacting with each other via the PPC/DUF296 domain. PNAS **110**: E4688–E4697.

Zhao J., Favero D.S., Qiu J., Roalson E.H., Neff M.M. (2014). Insights into the evolution and diversification of the *AT-hook Motif Nuclear Localized* gene family in land plants. BMC Plant Biol **14**: 1–19.

Zhao L., Lü Y., Chen W., Yao J., Li Y., Li Q., Pan J., Fang S., Sun J., Zhang Y. (2020). Genome-wide identification and analyses of the *AHL* gene family in cotton (*Gossypium*). BMC Genomics. doi: 10.1186/s12864-019-6406-6

Zhou Y., Zhang X., Chen J., Guo X., Wang H., Zhen W., Zhang J., Hu Z., Zhang X., Botella J.R., et al (2022). Overexpression of *AHL9* accelerates leaf senescence in *Arabidopsis thaliana*. BMC Plant Biol **22**: 1–12.

Zwack P.J., Robinson B.R., Risley M.G., Rashotte A.M. (2013). Cytokinin Response Factor 6 negatively regulates leaf senescence and is induced in response to cytokinin and numerous abiotic stresses. Plant Cell Phys **54**: 971–981.

Supplementary figures

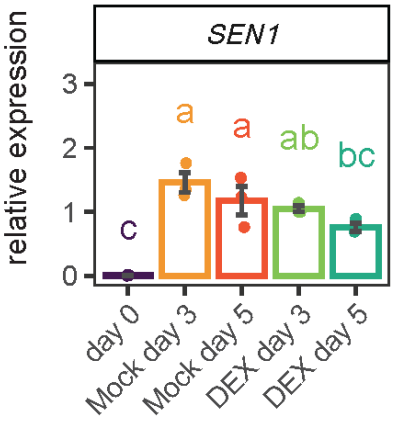

Supplementary figure 1. Expression of *SEN1* relative to *ACTIN2* in dark-incubated leaves with or without 10 µM DEX treatment. Expression was measured in three biological replicates (n=3) each composed of leaf material of three plants each. The Kruskall-Wallis test was used to compare conditions, and significance groups are indicated by different letters ($p < 0.05$).

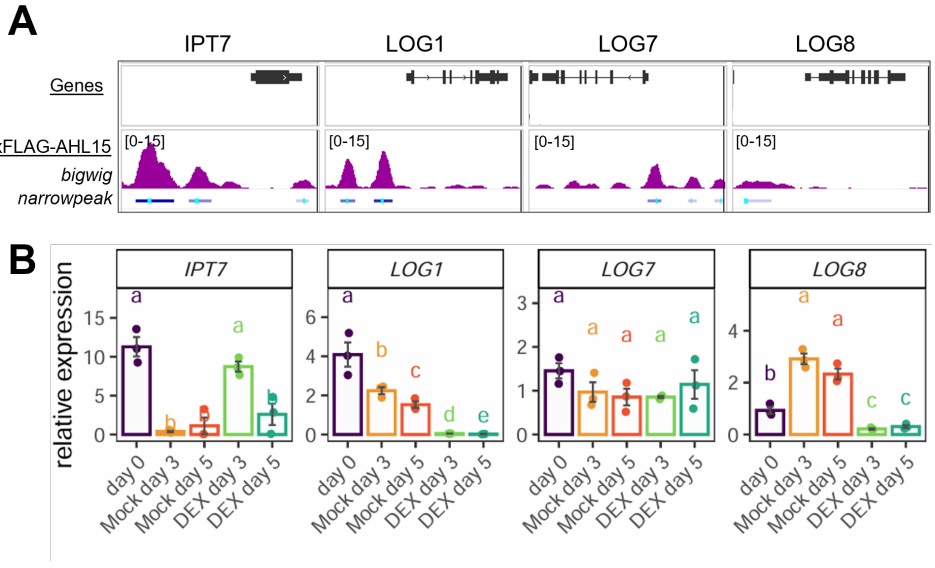

Supplementary figure 2. A: AHL15 binding to cytokinin biosynthesis genes *IPT7, LvvOG1, LOG7,* and *LOG8* in 31 day-old *AHL15* OX (*p35S:3xFLAG-AHL15*) plants using an anti-flag antibody to pull down AHL15-bound DNA. Signfiicant peaks were found at 1.4 kb and 3 kb upstream and in the 3' UTR of *IPT7,* at 1 kb and 2.1 kb upstream of *LOG1,* directly upstream of *LOG7,* and at 1.6 kb upstream of *LOG8.* The figure shows read alignment in purple (bigwig track), and the location of significant peaks in blue (narrowpeak track); a light blue bar indicates the peak summit. **B:** Expression of *IPT7, LOG1,LOG7,* and *LOG8* in the fifth leaf of 23-day old *35S:AHL15-GR* plants during dark-induced senescence with or without AHL15-GR induction by 10 µM DEX treatment. Expression was measured in three biological replicates (n=3) each composed of leaf material of three plants each. The Kruskall-Wallis test was used to compare conditions, and significance groups are indicated by different letters ($p < 0.05$).

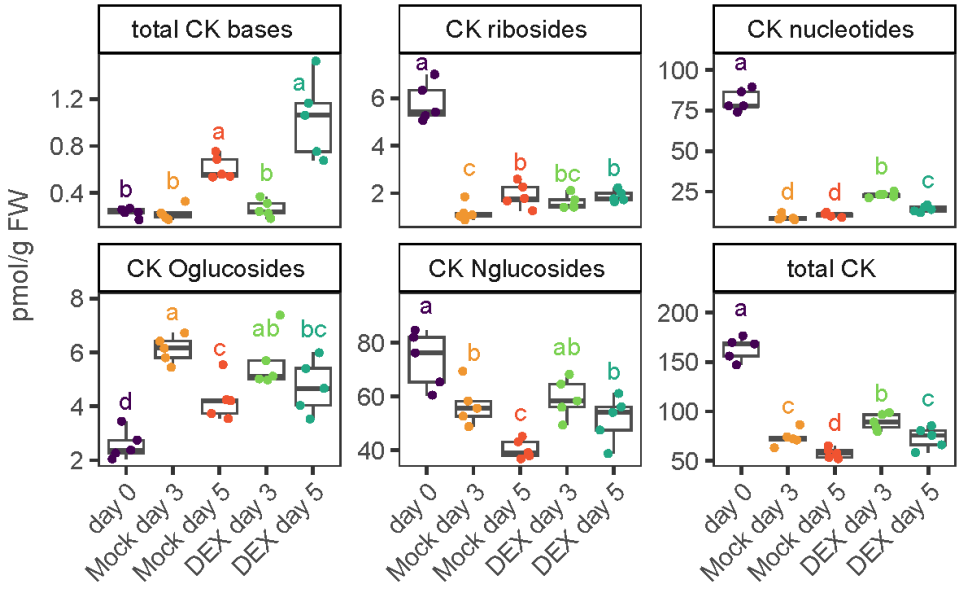

Supplementary figure 3. Effect of AHL15-GR induction on CK levels in dark-incubated leaves. The fifth leaf was collected from 23 days old plants and floated on 5 mM MES with or without 10 µM DEX and stored in the dark for the indicated number of days. Material of three leaves was pooled for each sample, and five samples were measured for each condition (n = 5). Groups were compared using the Kruskall-Wallis test, and letters indicate significance groups ($p < 0.05$).

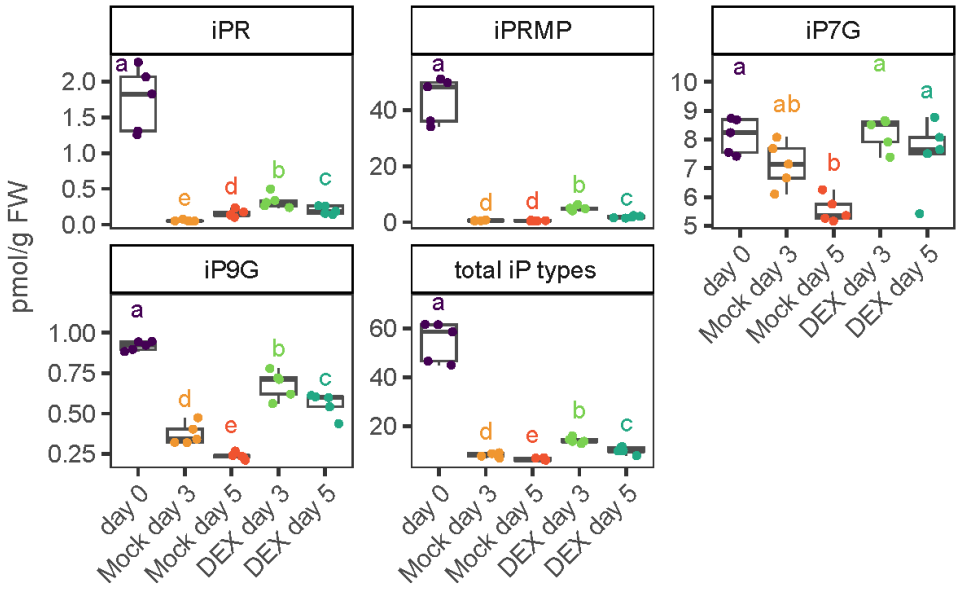

Supplementary figure 4. Effect of AHL15-GR induction on iP-derivatives in dark-incubated leaves. The fifth leaf was collected from 23 days old plants and floated on 5 mM MES with or without 10 μM DEX and stored in the dark for the indicated number of days. Material of three leaves was pooled for each sample, and five samples were measured for each condition (n = 5). Groups were compared using the Kruskall-Wallis test, and letters indicate significance groups ($p < 0.05$). iP base was not present at detectable levels.

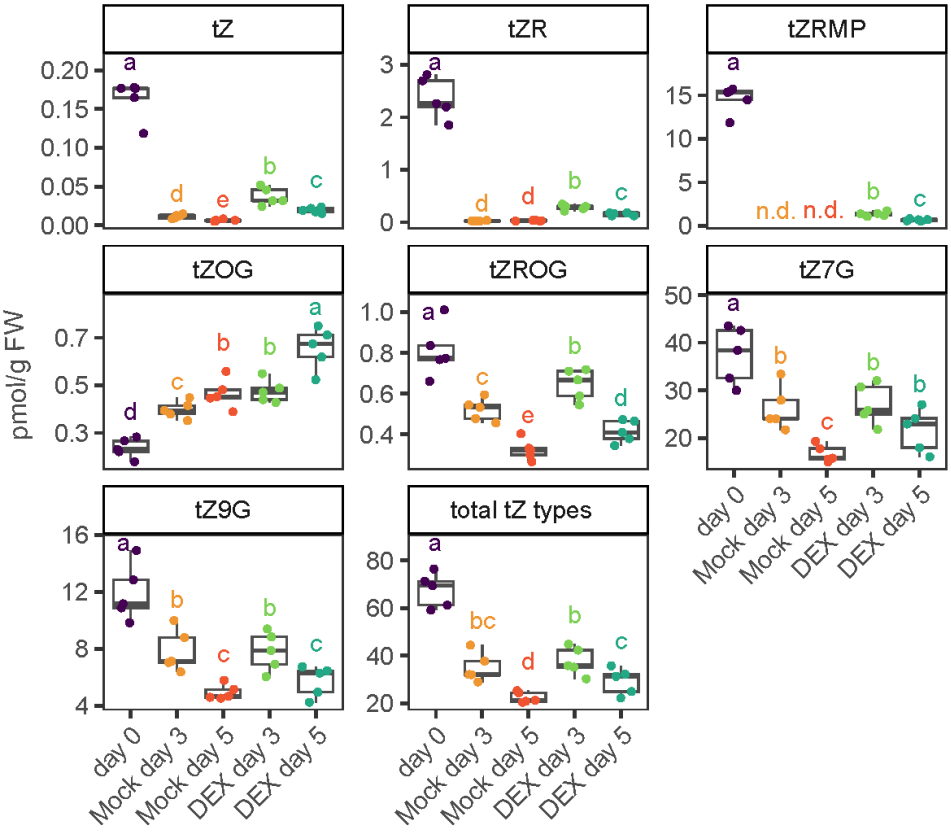

Supplementary figure 5. Effect of AHL15-GR induction on tZ and its derivatives in dark-incubated leaves. The fifth leaf was collected from 23 days old plants and floated on 5 mM MES with or without 10 µM DEX and stored in the dark for the indicated number of days. Material of three leaves was pooled for each sample, and five samples were measured for each condition (n = 5). Groups were compared using the Kruskall-Wallis test, and letters indicate significance groups ($p < 0.05$).

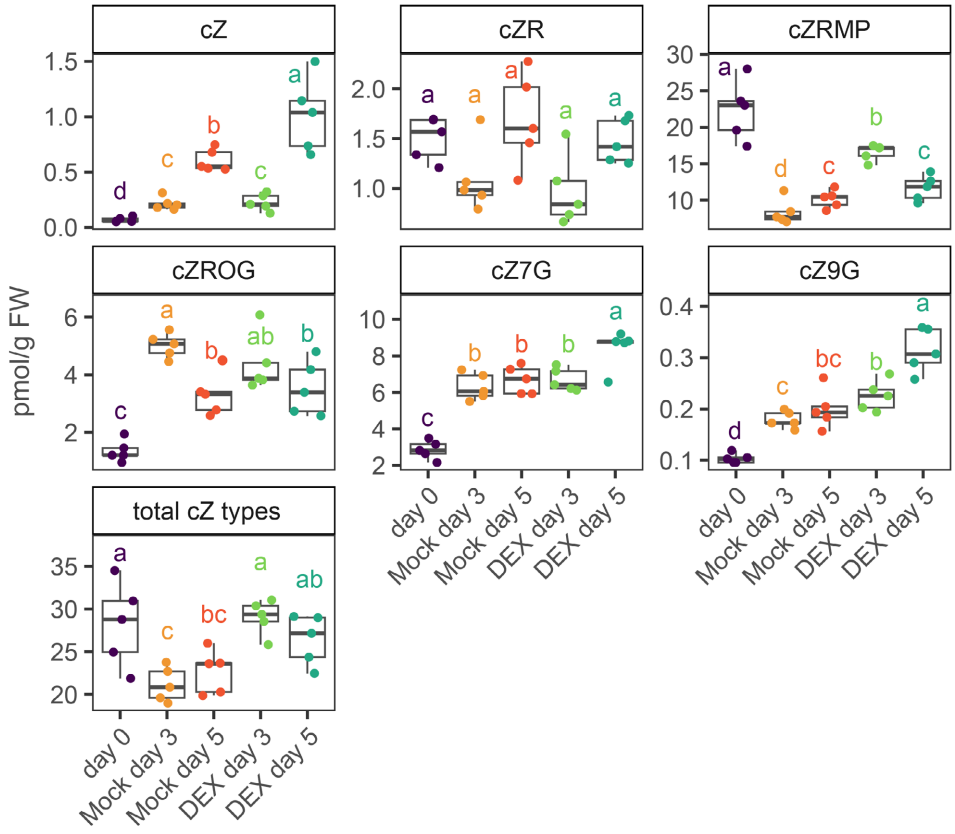

Supplementary figure 6. Effect of AHL15-GR induction on cZ and its derivatives in dark-incubated leaves. The fifth leaf was collected from 23 days old plants and floated on 5 mM MES with or without 10 μM DEX and stored in the dark for the indicated number of days. Material of three leaves was pooled for each sample, and five samples were measured for each condition (n = 5). Groups were compared using the Kruskall-Wallis test, and letters indicate significance groups ($p < 0.05$).

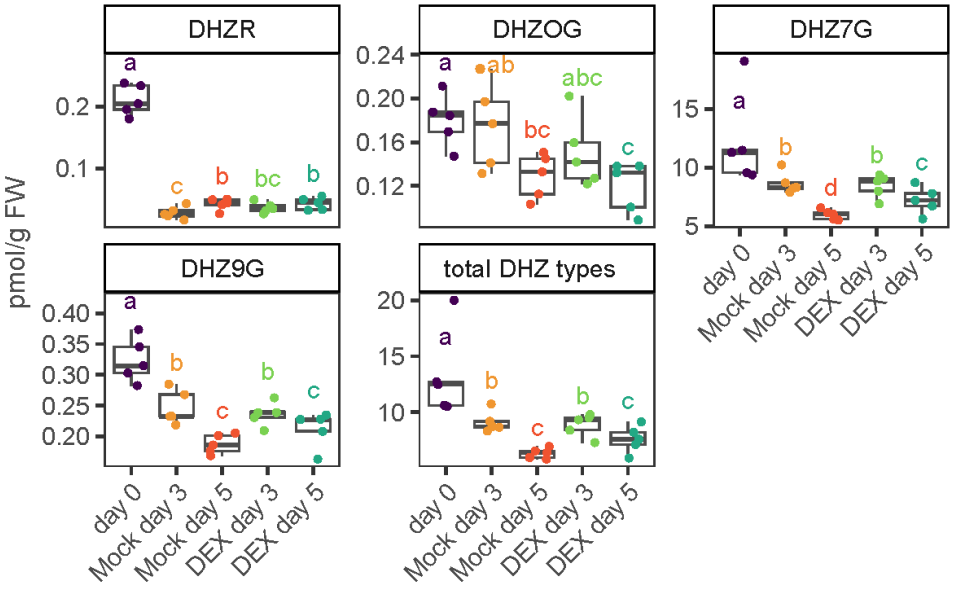

Supplementary figure 7. Effect of AHL15-GR induction on DHZ derivatives in dark-incubated leaves. The fifth leaf was collected from 23 days old plants and floated on 5 mM MES with or without 10 µM DEX and stored in the dark for the indicated number of days. Material of three leaves was pooled for each sample, and five samples were measured for each condition (n = 5). Groups were compared using the Kruskall-Wallis test, and letters indicate significance groups ($p < 0.05$). DHZ base was not present at detectable levels in these samples.

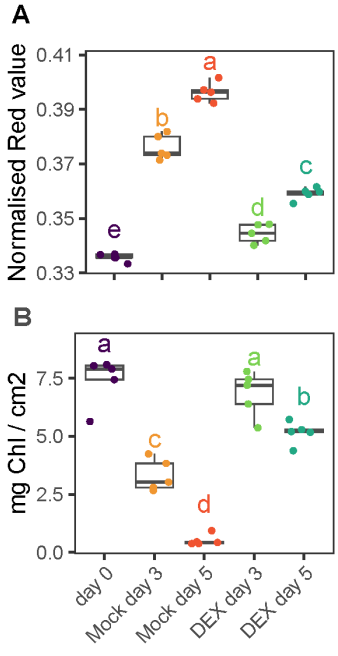

Supplementary figure 8. Quantification of senescence in leaves used for CK measurements. **A:** Normalized Red values (Rn) based on RGB images of leaves just before collecting material for CK measurements. **B:** Total chlorophyll content determined by acetone-based chlorophyll extraction in leaf disks taken from the same samples as used for CK measurements. For each condition, five samples were measured (n = 5), each consisting of material from the fifth leaf harvested from three individual plants. Groups were compared with the Kruskall-Wallis test, and letters indicate significance groups ($p < 0.05$).

Supplementary data

name	sequence (5' to 3')	function
ACTIN2-q-fw	TTCCTCAGCACATTCCAGCAGAT	reference gene for RT-qPCR
ACTIN2-q-rev	AACGATTCCTGGACCTGCCTCATC	reference gene for RT-qPCR
ORE1-q-fw	CTTACCATGGAAGGCTAAGATGGG	RT-qPCR of ORE1
ORE1-q-rev	TTCCAATAACCGGCTTCTGTCG	RT-qPCR of ORE1
SAG12-q-fw	ACCGGGACATCCTCATAACCTG	RT-qPCR of SAG12
SAG12-q-rev	ACAAAGGCGAAGACGCTACTTG	RT-qPCR of SAG12
SAG13-q-fw	AGGGAGCATCGTGCTCATATCC	RT-qPCR of SAG13
SAG13-q-rev	CCAGCTGATTCATGGCTCCTTTG	RT-qPCR of SAG13
SEN1-q-fw	GTTGTCGTTGCTTTCCTCCATC	RT-qPCR of SEN1
SEN1-q-rev	GTCATCGGCTATTTCTCCACCT	RT-qPCR of SEN1
CKX2-q-fw	GAGGTTTGGGTCAATTTGGA	RT-qPCR of CKX2
CKX2-q-rev	AGAGCATCCGAAACCATTTG	RT-qPCR of CKX2
CKX3-q-fw	TCTCAATACACAGTCAACGAGGA	RT-qPCR of CKX3
CKX3-q-rev	TCGTACATAAACCCTCTTACATGG	RT-qPCR of CKX3
CKX5-q-fw	CCATGGTCCTCAAATTAGTAACG	RT-qPCR of CKX5
CKX5-q-rev	TCTGAGCATCTCATCACCTCTC	RT-qPCR of CKX5
LOG1-q-fw	TTTTGTGGAAGTAGTGCTGGTAATA	RT-qPCR of LOG1
LOG1-q-ref	AAATCAAACCCATTAAACCAAT	RT-qPCR of LOG1
LOG2-q-fw	ACACTAAACCGGTGGGACTATTGAA	RT-qPCR of LOG2
LOG2-q-rev	GGAGCGTTTGGAGCCGAGAC	RT-qPCR of LOG2
LOG7-q-fw	CGCTGTTAACGTTTATTGATAAGGC	RT-qPCR of LOG7
LOG7-q-rev	TTATCTCATCAAACTCCGGTTCA	RT-qPCR of LOG7
LOG8-q-fw	GTTTATGGAGGAGGAAGTGTTGGAT	RT-qPCR of LOG8
LOG8-q-rev	TCACCAGATATCTCAATTGGCAT	RT-qPCR of LOG8
IPT7-q-fw	ACCTAACGGCCACCCAGTAT	RT-qPCR of IPT7
IPT7-q-rev	CGGAGTAATTCGCTTTTGGA	RT-qPCR of IPT7
	* fw: forward, rev: reverse	

Supplementary table 1: Primers used for RT-qPCR in this study.